Phase Noise of Pulse Injection-Locked Oscillators

Paolo Maffezzoni, *Member, IEEE*, and Salvatore Levantino, *Member, IEEE*

I. Introduction

THE combination of injection locking with conventional methods for frequency synthesis, such as the phase-locked loop (PLL), is a promising solution for the design of high-performance clock multipliers and frequency synthesizers [1]–[4]. In fact, the superior suppression of the oscillator phase noise provided by the injection-locking mechanism compared to that provided by the PLL allows one to get frequency synthesizers with lower phase noise at lower power.

Injection-locked oscillators to be used in such a context need to be locked to a sub-harmonic of their own oscillation frequency and for this reason, they are typically implemented as pulse injection-locking oscillators (PILOs).[1] A PILO is an oscillatory circuit which is injected with a stream of narrow pulses generated from the reference signal. If the free-running frequency of the oscillator is sufficiently close to the Nth harmonic of the reference, with N being the multiplication factor, the oscillator will lock to that harmonic according to a nonlinear dynamic phenomenon and its average frequency will become N times the reference frequency. Injection locking forces the oscillator to follow the reference frequency thus attenuating phase-noise effects. Of course, the achievable phase-noise reduction depends on numerous factors and design parameters such as the shape, the power and the frequency of the injected pulses as well as the desired multiplication factor N. Predicting phase noise of PILO circuits by means of transistor-level simulations requires to run, for each parameter setting, several periodic steady state and periodic noise analyses with commercial simulation tools. As a result, the exploration of several potential parameter settings becomes prohibitively time consuming for large multiplication factor N values and as the circuit complexity increases.

A much more efficient approach consists in the adoption of oscillator macromodels [7]–[10]. Nevertheless, widely adopted phase-domain macromodels based on oscillator linearization around its stable orbit, e.g., those based on Perturbation Projection Vector (PPV) [8] or Impulse Sensitivity Function (ISF) [9], are valid only under weak injected signals and are not suitable to describe the injection locking mechanism in a PILO [11]–[15]. This is because injected pulses are large-amplitude perturbations that cause large deviations from the free-running orbit.

For these reasons, in this paper we employ an extended macromodeling methodology which is able to deal with the case of large-amplitude pulse injection. The concept of large-signal phase-response has been first introduced in modeling spiking biological oscillators in neuroscience [14] and only very recently it has been applied to the analysis of electronic oscillators [15]. In this paper, for the first time we use this novel paradigm to quantify phase noise in sub-harmonic PILOs.

Our Contribution. The novel contributions of our paper over existing literature can be summarized as follows:

1) We use the above described concept of large-signal phase-response to derive a noise-aware model of PILO. This model is given by a stochastic nonlinear equation that describes the time evolution of the excess phase at discrete-time points.
2) By exploiting the fact that the phase fluctuations around the locked value due to PILO internal noise sources are small, we provide an original closed-form expression of phase noise.
3) We describe an efficient computational procedure which allows us to quantify PILO phase noise as a function of the main design parameters.

Paper Organization. Section II formalizes the concept of large-signal phase-response and introduces the PILO model. In Section III, we outline the noise-aware PILO model while in Section IV we derive the closed-form expression for the PILO output phase noise. Section V illustrates the application of the novel methodology to the analysis of a PILO topology.

II. Pulse Injection Locking

Fig. 1-(Left) shows the circuit of a PILO based on an LC tank oscillator. The injected voltage pulse train can be represented mathematically by the following expression

$$v_{inj}(t) = s(\omega_{inj} t + \theta_{inj}), \tag{1}$$

Manuscript received December 13, 2013; revised February 08, 2014 and April 11, 2014; accepted April 17, 2014. Date of publication May 09, 2014; date of current version September 25, 2014. This paper was recommended by Associate Editor N. M. Neihart.

The authors are with the Dipartimento di Elettronica, Informazione e Bioingegneria, Politecnico di Milano, 20133 Milan, Italy (e-mail: pmaffezz@elet.polimi.it; levantin@elet.polimi.it).

[1]Other ways to achieve frequency multiplication exist in the literature, e.g array of coupled oscillators [5], [6], but they will not be considered in this paper.

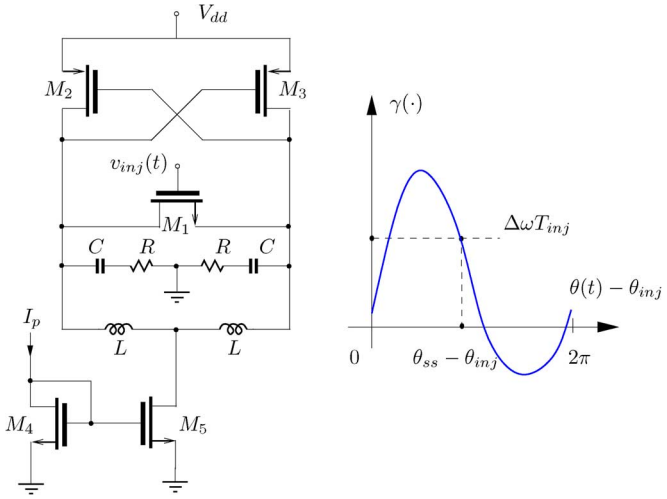

Fig. 1. (Left) LC-type PILO circuit. (Right) A qualitative example of PDR $\gamma(\cdot)$: the curve gives the amount of PILO phase variation induced by a single pulse over one reference period as a function of the initial phase value (compared to that of the reference). Sub-harmonic injection locking occurs at θ_{ss} where the curve intersects the value $\Delta\omega T_{inj}$ with a negative slope.

where $s(\cdot)$ is a 2π-periodic function of its instantaneous phase $\omega_{inj}t + \theta_{inj}$, while ω_{inj} and $T_{inj} = 2\pi/\omega_{inj}$ are the injection (angular) frequency and period respectively and θ_{inj} is an initial constant phase. The injected voltage controls the gate of the transistor M_1, which is off for most of the time and on at each pulse of $v_{inj}(t)$. In practice, a resistance of low value shorts periodically the voltage across the LC resonator. The frequency ω_{inj} of the shorting pulse train, which is the same as the reference frequency, is set to a sub-multiple N of the desired output frequency, while the width of the pulses is commonly set to be much less than the oscillation period.

The voltage across the resonator of the unperturbed oscillator can be written as $v_0(t) = p(\omega_0 t)$, where $\omega_0 = 2\pi f_0$ is the free-running oscillation frequency and $p(\cdot)$ is a 2π-periodic function of instantaneous phase $\omega_0 t$. Injection locking can occur only if the injection frequency ω_{inj} is close to ω_0/N or alternatively if the relationship $\omega_0 + \Delta\omega = N\omega_{inj} = \omega_{lock}$ holds, where $|\Delta\omega| \ll \omega_0$ is a sufficiently small frequency detuning and ω_{lock} is the frequency of the locked oscillator.

Let us consider one reference period starting at $t_1 = 0$ and ending at $t_2 = T_{inj}$. The phase variation of the injected signal (1) over one period is clearly zero (a multiple of 2π is equivalent to zero due to the periodicity of $s(\cdot)$). Indeed, the phase variation of the free-running response over a reference period is

$$\omega_0 t_2 - \omega_0 t_1 = -\frac{\Delta\omega 2\pi}{\omega_{inj}} = -\Delta\omega T_{inj}. \tag{2}$$

We thus conclude that, in the absence of injection, during one reference period the phase of the free-running oscillator would be shifted by the value $-\Delta\omega 2\pi/\omega_{inj}$ with respect to that of the injected signal.

In a PILO circuit, the application of pulses of large amplitude and short duration (compared to T_0) produces both amplitude and phase variations in the response with respect to the free-running one. Due to the intrinsic amplitude limiting mechanism, the amplitude variation produced by a single pulse is rapidly attenuated by the PILO dynamics and it can be considered damped to zero before the application of the next pulse (which occurs after a long time interval $\approx N \times T_0$). By contrast, due to the neutral stability of the phase response, the phase variations induced by the injected pulses are accumulated in time with no attenuation. As a consequence, to the aim of studying injection locking mechanism, PILO response can be properly described by the following phase-domain model

$$v_{PILO}(t) = p\left[(\omega_0 + \Delta\omega)t + \theta(t)\right] = p\left[\omega_{lock}t + \theta(t)\right], \tag{3}$$

where $\theta(t)$ represents the phase deviation from the desired locked value $\omega_{lock}t$.

The application of each single pulse over one reference period will produce, as a response, a variation of the phase variable $\theta(t)$ the amount of which will depend, in turn, on the value of $\theta(t)$ compared to the phase of the reference signal. This behavior can be formalized mathematically as follows

$$\theta(t + T_{inj}) - \theta(t) = \gamma\left(\theta(t) - \theta_{inj}\right) \tag{4}$$

where $\gamma(\cdot)$ denotes the periodic function that describes the time-varying sensitivity of the phase response. Fig. 1-(Right) shows the qualitative shape of the $\gamma(\cdot)$ function.

This function has been introduced in different contexts with different names: in [14] it was referred to as Phase Response Curve (PRC), while in [15] it was denoted as Phase Domain Response (PDR). The numerical computation of $\gamma(\cdot)$ which is described in Appendix A entails simulating the transient responses (over one injection period) of the oscillator after the injection of a single pulse. The application time of the pulse is gradually shifted over the oscillation period and the transient analysis is repeated.

We treat now each period of the injected signal as a *discrete time event* and we denote as $\theta(t_k)$ the phase variable $\theta(t)$ of the PILO circuit, measured at the beginning of the kth injection. Considering both the phase delay (2) accumulated by the PILO when running freely and the phase shift (4) induced by one-pulse injection, we write

$$\theta(t_{k+1}) = \theta(t_k) + \gamma\left[\theta(t_k) - \theta_{inj}\right] - \Delta\omega T_{inj}. \tag{5}$$

The nonlinear model (5) governs the evolution of the phase variable $\theta(t_k)$ at the discrete time points t_k. Injection locking will occur when the phase deviation reaches the equilibrium value $\theta(t_k) = \theta_{ss}$ such that $\theta(t_{k+1}) = \theta(t_k) = \theta_{ss}$. By imposing the above equilibrium condition into (5), we get

$$\gamma(\theta_{ss} - \theta_{inj}) = \Delta\omega T_{inj}. \tag{6}$$

Condition (6) along with the shape of the $\gamma(\cdot)$ function shown in Fig. 1-(Right) tell a lot about the synchronizability of a PILO. In fact, for a given value of the frequency detuning $\Delta\omega$, injection locking will occur in correspondence to the phase difference value $\theta(t) - \theta_{inj} = \theta_{ss} - \theta_{inj}$ where $\gamma(\cdot)$ intersects $\Delta\omega T_{inj}$. Moreover, this locking condition will be stable only if the slope of the curve at the intersection point is negative. This can be seen with the help of (5): if the curve slope is negative, a positive initial perturbation of $\theta(t_k)$ (with respect to the lock value θ_{ss}) results in a reduction of the $\gamma(\cdot)$ term on the right-hand-side of (5) and thus compensates the initial perturbation. Vice versa, if the curve slope is positive, a positive perturbation of $\theta(t_k)$ induces an increase of $\gamma(\cdot)$ and makes $\theta(t_{k+1})$ run away from the locked state. Using the portion of the $\gamma(\cdot)$ function where its slope is negative, it is possible to invert the function so as to express the locked phase variable $\theta_{ss} - \theta_{inj}$ as a function of frequency detuning, i.e.,

$$\theta_{ss} - \theta_{inj} = g(\Delta\omega) = \gamma^{-1}(\Delta\omega T_{inj}). \tag{7}$$

Finally, the upper and lower limits γ_{max} and γ_{min}, respectively, of the curve $\gamma(\cdot)$ determine the locking range:

$$\frac{\gamma_{min}}{T_{inj}} \leq \Delta\omega \leq \frac{\gamma_{max}}{T_{inj}}. \tag{8}$$

III. Phase-Noise Model

In this section, we model the phase noise of the PILO circuit. To do this, we first review the phase-noise model of the free-running oscillator. To include phase in the model of the free-running oscillator, the expression of the output response is modified into $v_0(t) = p[\omega_0 t + \phi_n(t)]$, where $\phi_n(t)$ represents the excess phase induced by the internal noise sources of the oscillator. A compact modeling strategy can be used by exploiting the result derived in [16]: The total phase-noise contribution of all the oscillator internal noise sources of one type (i.e., characterized by its spectral characteristics) can be represented, in an equivalent way, by a single macro noise source of the same type as the input to an ideal integrator. Thus, the global effect that all the white and the flicker noise sources have on the oscillator phase variable $\phi(t)$ can be modelled through the following average stochastic equation [16]–[18]

$$\phi_n(t) = \omega_0 \int_{-\infty}^{t} n_{eq}(\tau)d\tau = \omega_0 \int_{-\infty}^{t} \left[n_w(\tau) + n_f(\tau)\right] d\tau. \tag{9}$$

In (9), $n_w(t)$ is the macro noise source with a constant Power Spectral Density (PSD) $S_w(f) = A_w$ which reproduces the effect of intrinsic white sources, while $n_f(t)$, with PSD $S_f(f) = A_f/f$, is the macro noise source that reproduces the global effect of intrinsic flicker noise sources. Hence, by transforming (9) in the frequency domain, we find that the PSD of the excess phase variable for the free-running oscillator has the expression

$$S_{\phi_n}(f) = f_0^2 \cdot \left(\frac{A_w}{f^2} + \frac{A_f}{f^3}\right), \tag{10}$$

and exhibits two components shaped as $1/f^2$ and $1/f^3$. The parameters A_w and A_f of the macro noise sources are extracted from the phase-noise spectrum of the free-running oscillator [19].

When the oscillator is injection locked, the internal noise sources produce an excess-phase fluctuation $\phi(t)$ of the variable $\theta(t)$ around its noiseless locking value, i.e., $\theta(t) = \theta_{ss} + \phi(t)$. Plugging the latter into the discrete-time model (5) and therein adding the phase variations induced by stochastic fluctuations (9) over one reference period, we obtain

$$\phi(t_{k+1}) = \phi(t_k) + \gamma\left(\theta_{ss} + \phi(t_k) - \theta_{inj}\right) - \Delta\omega T_{in} + \omega_0 \int_{t_k}^{t_{k+1}} n_{eq}(\tau)d\tau. \tag{11}$$

The nonlinear stochastic discrete-time (11) can be simulated in time to calculate the evolution of the excess phase variable $\phi(t_k)$ at time points t_k induced by PILO internal noise sources.

IV. Small-Signal Phase-Noise Analysis

In this section, instead, we will proceed analytically to find closed-form expressions of PILO phase noise. To this aim, the nonlinear stochastic difference (11) is simplified by exploiting the evidence that noise sources in a PILO generate small-amplitude signals and thus the excess-phase fluctuations $\phi(t_k)$ around θ_{ss} should remain small as well. The validity of this ansatz will be verified at the end of Section V.

Under this hypothesis, the $\gamma(\theta_{ss} - \theta_{inj} + \phi(t_k))$ function can be linearized around the locking phase value $(\theta_{ss} - \theta_{inj})$ so that the difference (11) is transformed to

$$\phi(t_{k+1}) \approx \phi(t_k) + \gamma(\theta_{ss} - \theta_{inj}) + \gamma'(\theta_{ss} - \theta_{inj})\phi(t_k) - \Delta\omega T_{inj} + \omega_0 \int_{t_k}^{t_{k+1}} n_{eq}(\tau)d\tau \tag{12}$$

where $\gamma'(\cdot)$ denotes the first derivative of the PDR curve $\gamma(\cdot)$ with respect to its argument.

Next, using the equilibrium condition (6), (12) is rewritten as

$$\phi(t_{k+1}) = \phi(t_k) - \beta(\Delta\omega)\phi(t_k) + \omega_0 \int_{t_k}^{t_{k+1}} n_{eq}(\tau)d\tau, \tag{13}$$

where the (positive) parameter

$$\beta(\Delta\omega) = -\gamma'(\theta_{ss} - \theta_{inj}) = -\gamma'\left[g(\Delta\omega)\right] \tag{14}$$

is the module of the slope of $\gamma(\cdot)$ evaluated at locking phase condition. This parameter measures the responsivity of the PILO to perturbations of the locking phase. In view of (7), this parameter depends on the value of the frequency detuning. However, for notation simplicity, in what follows the dependence of β on $\Delta\omega$ will be omitted.

A continuous-time model can then be obtained by writing the difference (13) over the infinite series of sample points $-\infty, \ldots, t_k, t_{k+1}$ with $t_k = k \cdot T_{inj}$, i.e.

$$\begin{aligned}
\phi(t_{k+1}) - \phi(t_k) &= -\beta\phi(t_k) + \omega_0 \int_{t_k}^{t_{k+1}} n_{eq}(\tau)d\tau \\
\phi(t_k) - \phi(t_{k-1}) &= -\beta\phi(t_{k-1}) + \omega_0 \int_{t_{k-1}}^{t_k} n_{eq}(\tau)d\tau \\
&\ldots
\end{aligned} \tag{15}$$

Adding the above equations together and assuming $\phi(-\infty) = 0$ and $t = t_{k+1}$, we get

$$\phi(t) = -\beta \sum_{j=-\infty}^{k} \phi(t_j) + \omega_0 \int_{-\infty}^{t} n_{eq}(\tau)d\tau, \tag{16}$$

or, equivalently, in compact form

$$\phi(t) = -\beta \int_{-\infty}^{t} \phi(\tau) \sum_k \delta(\tau - t_k)d\tau + \phi_n(t). \tag{17}$$

In the expression above, "$\sum_k$" stands for "$\sum_{k=-\infty}^{\infty}$," symbol $\delta(t)$ denotes the Dirac delta distribution, while $\phi_n(t)$ is the phase noise of the free-running PILO circuit. The integral in (17) can be rewritten as a convolution integral, i.e.

$$\phi(t) = -\beta \int_{-\infty}^{\infty} \phi(\tau) \sum_k \delta(\tau - t_k)h(t - \tau)d\tau + \phi_n(t). \tag{18}$$

where $h(t) = \mathrm{sca}(t - \Delta)$ is the unit step function delayed by any Δ such that $0 < \Delta \leq T_{inj}$. Such a delay is in fact needed to correctly implement (16) where the summation of excess phase samples stops at $\phi(t_k)$. Since Δ is arbitrarily distributed in the

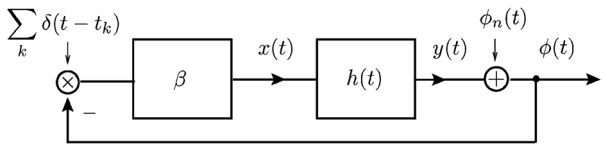

Fig. 2. Variational time-domain model of the PILO.

interval $(0, T_{inj})$, in solving (18) we will fix it to its mean value $\Delta = T_{inj}/2$.

To solve (18) it is convenient to represent it graphically as the block diagram shown in Fig. 2. In this representation, the convolution integral is performed by the linear block with impulse response $h(t)$ and transfer function

$$H(f) = \frac{1}{j2\pi f} \exp(-j\pi f T_{inj}). \tag{19}$$

This linear block reads in input the variable

$$x(t) = -\beta \cdot \phi(t) \sum_k \delta(t - t_k) \tag{20}$$

and supplies the output $y(t) = x(t) * h(t)$ where "$*$" denotes convolution operation.

From the graphical representation in Fig. 2 and the definition of $x(t)$, we therefore derive an alternative expression of (18), which is given by the two following equations

$$\phi(t) = x(t) * h(t) + \phi_n(t) \tag{21}$$

$$[(x(t) * h(t) + \phi_n(t))] \cdot (-\beta) \sum_k \delta(t - t_k) = x(t). \tag{22}$$

The latter can be rewritten as

$$-\beta \cdot (x(t) * h(t)) \cdot \sum_k \delta(t - t_k) - \beta \cdot \sum_k \phi_n(t_k) \delta(t - t_k) = x(t). \tag{23}$$

The first term in (23) can be further expanded by exploiting the fact that the result does not change if the order of application of convolution "$*$" and multiplication "$\cdot$" operators on the train of pulses is inverted. Inverting this order, we find

$$-\beta \cdot x(t) * \left(\sum_k h(t_k) \delta(t - t_k) \right) - \beta \cdot \sum_k \phi_n(t_k) \delta(t - t_k) = x(t). \tag{24}$$

By Fourier transforming both sides of (24) and remembering (19), we find

$$-X(f) \frac{\beta}{T_{inj}} \cdot \sum_k \frac{\exp\left[-j\pi \left(f - \frac{k}{T_{inj}}\right) T_{inj}\right]}{j2\pi \left(f - \frac{k}{T_{inj}}\right)} - \frac{\beta}{T_{inj}} \cdot \sum_k \Phi_n \left(f - \frac{k}{T_{inj}}\right) = X(f) \tag{25}$$

where $X(f)$ and $\Phi_n(f)$ are the Fourier transforms of $x(t)$ and $\phi_n(t)$, respectively. Solving (25) in the unknown $X(f)$ gives

$$X(f) = -\sum_k \Phi_n \left(f - \frac{k}{T_{inj}}\right) \cdot T(f) \tag{26}$$

having $T(f)$ the following expression

$$T(f) = \frac{\frac{\beta}{T_{inj}} \frac{1}{j2\pi f}}{1 + \frac{\beta}{T_{inj}} \sum_k \frac{\exp\left[-j\pi \left(f - \frac{k}{T_{inj}}\right) T_{inj}\right]}{j2\pi \left(f - \frac{k}{T_{inj}}\right)}}. \tag{27}$$

The sum of the series at the denominator of (27) has an analytical closed-form expression which is derived in the Appendix B. Relying on that result, $T(f)$ can be simplified as follows

$$T(f) = \frac{\beta}{\beta \pi f T_{inj} \cdot \mathrm{cotg}(\pi f T_{inj}) + j\pi f T_{inj}(2 - \beta)}. \tag{28}$$

By Fourier transforming both sides of (21), we get the relationship between the output spectrum of the PILO circuit and $X(f)$

$$\Phi(f) = X(f) \cdot H(f) + \Phi_n(f) \tag{29}$$

where $\Phi(f)$ is the Fourier transform of $\phi(t)$. Thus, replacing (26) into (29) and reordering the terms, we get

$$\Phi(f) = \Phi_n(f) \cdot [1 - T(f)] - \left(\sum_{k, k \neq 0} \Phi_n \left(f - \frac{k}{T_{inj}}\right) \right) \cdot T(f). \tag{30}$$

From the above expression, the excess phase PSD $S_\phi(f)$ of the PILO circuit is found to be composed of the two contributions

$$S_\phi(f) = S_\phi^D(f) + S_\phi^F(f). \tag{31}$$

The first one

$$S_\phi^D(f) = S_{\phi_n}(f) \cdot |1 - T(f)|^2 \tag{32}$$

describes how the phase noise $S_{\phi_n}(f)$ of the free-running oscillator is directly transferred to the output of the PILO. The second contribution

$$S_\phi^F(f) = \left(\sum_{k, k \neq 0} S_{\phi_n} \left(f - \frac{k}{T_{inj}}\right) \right) \cdot |T(f)|^2 \tag{33}$$

is due to the folded power spectrum. This spectrum folding arises from the sub-sampling of noise operated by pulse injection.

The nature of the above spectral components can be better understood by approximating (28) at low and high frequencies. At frequencies approaching zero, or in practice at frequencies much lower than the injection frequency $f_{inj} = 1/T_{inj}$, from (28) we can approximate the two components of the noise spectrum as

$$S_\phi^D(f) \approx \pi^2 N^2 \left(\frac{2}{\beta} - 1\right)^2 \left(A_w + \frac{A_f}{f}\right)$$

$$S_\phi^F(f) \approx \pi^2 N^2 \frac{A_w}{3} + 2.4 T_0 N^3 A_f. \tag{34}$$

When flicker is negligible (i.e., for frequency offsets above flicker corner), from (34) we infer that the in-band total noise is flat and approaches the power spectral density value given by

$$\lim_{f \to 0} S_\phi(f) \approx \pi^2 N^2 \left[\left(\frac{2}{\beta} - 1\right)^2 + \frac{1}{3} \right] A_w. \tag{35}$$

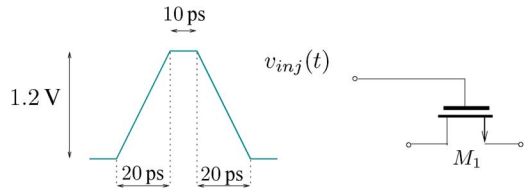

Fig. 3. The shape of the injected voltage pulse.

Expression (35) highlights the parameters of the macromodel that mainly affect the level of in-band noise (at offset frequencies lower than f_{inj}). These parameters are: the intensity of internal noise sources A_w defined in (10), the PILO parameter β defined in (14) and the multiplication factor N. At frequencies much greater than f_{inj}, the two noise transfer functions in (32) and (33) approach the following limit values $\lim_{f\to\infty}|T(f)|^2 = 0$ and $\lim_{f\to\infty}|1-T(f)|^2 = 1$. Thus, the direct contribution $S_\phi^D(f)$ to the output spectrum tends to that of the free-running oscillation $S_{\phi_n}(f)$. This is consistent with the fact that the locking process is ineffective at large offset frequencies. Notwithstanding, our model predicts the existence of the additional contribution $S_\phi^F(f)$, due to power spectrum folding and defined in (33), that yields a ripple in the noise spectrum at frequencies close to multiples of f_{inj}. The amount of this high-frequency extra noise contribution will be evaluated in Section V.

V. Numerical Results

In this section, the proposed phase-noise analysis methodology is applied to the circuit in Fig. 1-(Left). The device parameters are: $V_{dd} = 1.2$ V, $I_p = 4.5$ mA, $C = 2.5$ pF, $L = 1$ nH, $R = 2\ \Omega$, $(W/L)_{2,3} = 20/0.06$, and $(W/L)_{4,5} = 10/0.06$. The steps of the analysis are described in what follows.

First, the free-running oscillator is simulated with Cadence SpectreRF [21]. The waveform of its output voltage $v_0(t)$ resulting from periodic steady state (*pss*) analysis is an oscillation with peak-to-peak amplitude of about 1.9 V, angular frequency $\omega_0 = 2\pi \times 3.1982 \cdot 10^9$ rad/s and period $T_0 = 312.68$ ps. Using the periodic noise analysis (*pnoise*) of SpectreRF, the phase-noise spectrum $S_{\phi_n}(f)$ of the free-running oscillator is extracted. By fitting this noise spectrum with (10), we extract the equivalent noise parameters $A_w = 8.7 \cdot 10^{-20}$ rad^2/Hz and $A_f = 4.5 \cdot 10^{-19}$ rad^2. Next, we apply the injected voltage signal $v_{inj}(t)$, whose shape is schematically shown in Fig. 3. The peak value of the injected signal is fixed to the voltage supply value V_{dd}, whereas the strength of the injection is modulated by varying the width W_1 of the injecting transistor M_1. The corresponding $\gamma(\cdot)$ curves, extracted with the method described in the Appendix A, are shown in Fig. 4. According to (8), the upper and lower limits of these curves, for several values of parameter W_1, determine the synchronization region plotted in Fig. 5 (commonly referred to as Arnold tongue [20]). The slope of the curves $\gamma(\cdot)$ (evaluated at the intersection with the locking condition $\Delta\omega T_{inj}$) gives the value of the parameter $-\beta(\Delta\omega)$ defined in (14) and plotted in Fig. 6 as a function of $\Delta\omega$ and for $N = 10$.

The values of β are then substituted in (28) to get the expression of the transfer function $T(f)$ and the phase noise is evaluated through the closed-form expressions from (31) to (33). Fig. 7 shows the direct $S_\phi^D(f)$ and folded $S_\phi^F(f)$ spectral components, respectively, for $N = 10$, $\Delta\omega \approx 0$ and

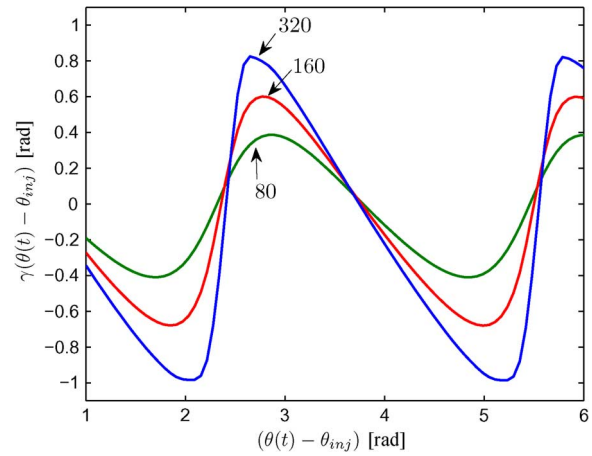

Fig. 4. Computed PDR $\gamma(\cdot)$ functions for three values of the parameter W_1 (measured in μm).

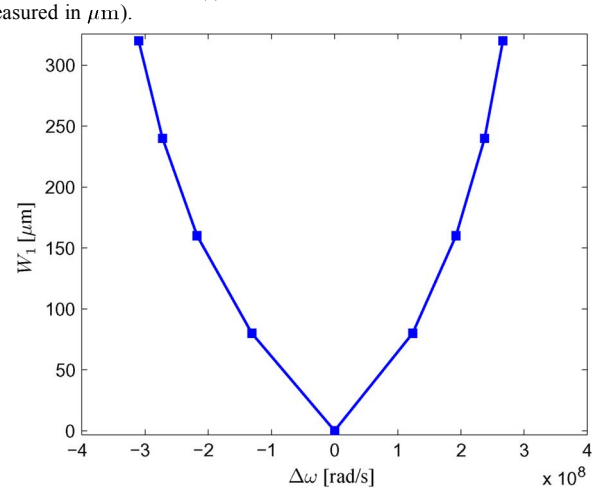

Fig. 5. Synchronization region.

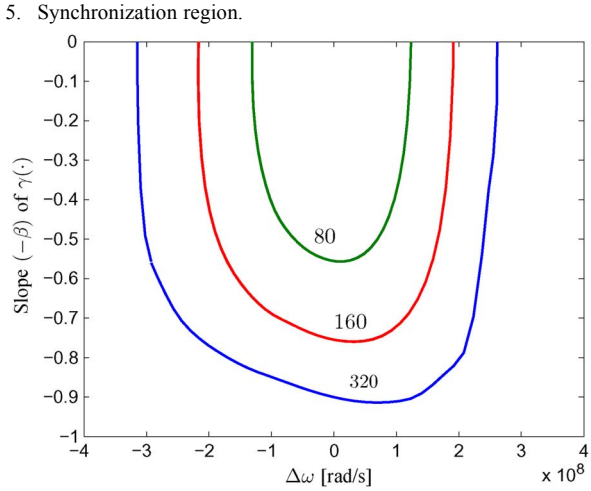

Fig. 6. Slope $-\beta$ as a function of the frequency detuning for three values of the parameter W_1 (measured in μm).

$W_1 = 320$ μm. The direct noise contribution $S_\phi^D(f)$ dominates the output power spectrum at low frequencies while the folded noise defined in (33) adds a non-negligible ripple component at high frequencies. The total phase-noise spectrum $S_\phi(f)$ given by the sum of the two previous contributions is also shown in the same figure (solid line). For the same set of parameters, the PILO circuit is simulated with SpectreRF. A *pss* analysis based on the flexible balance algorithm is performed with beat frequency equal to $1/T_{inj} = 1/(T_0 \times N)$ and with 256

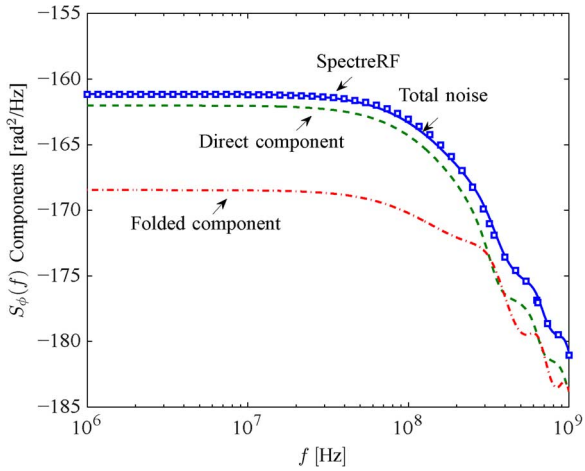

Fig. 7. Phase noise of the PILO circuit for $W_1 = 320\ \mu$m and $N = 10$: (dashed line) direct component $S_\phi^D(f)$ from (32), (dot-dashed line) folded component $S_\phi^F(f)$ from (33), (solid line) total noise from theory, (square markers) simulated noise from SpectreRF.

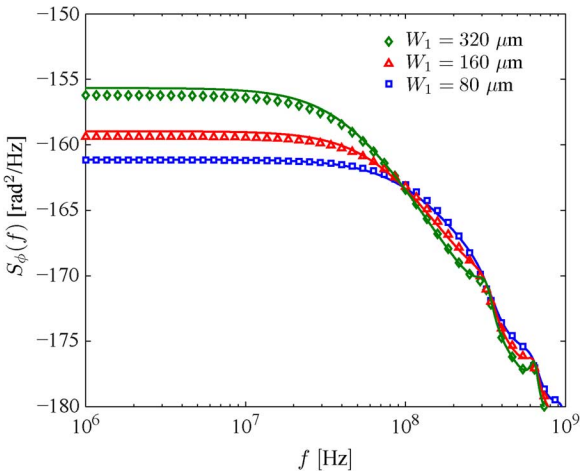

Fig. 8. Phase noise of the PILO circuit for $N = 10$ and the three values 80, 160, and 320 μm (from top to down) of the W_1 parameter: (solid lines) noise from theory (markers) simulated noise from SpectreRF.

harmonics. The high number of harmonics is needed because of the high N factor between the beat frequency and the oscillation frequency of the PILO circuit. Then, a *pnoise* analysis is run accounting for 128 harmonics. The phase noise obtained is shown as square markers in Fig. 7. Simulations and theory match very well.

To validate further the proposed analysis, we repeat the same comparison at different values of the circuit parameters. First, we change the width of the injection transistor W_1. Fig. 8 plots the phase noise obtained for $N = 10$ and the three values 80, 160, and 320 μm of W_1 parameter. Of course, a lower W_1 results in a narrower noise-filtering bandwidth and, in turn, in a higher level of in-band noise. Even for these sets of parameters, the simulated points from SpectreRF, also shown in Fig. 8, match the theoretical prediction.

Fig. 9 plots the phase noise for $W_1 = 320\ \mu$m and several values of the multiplication factor N from 10 to 160. The values of the other parameters are kept constant. So, as N increases, the frequency of the injected pulse train is scaled down, while the output frequency is constant. The analytical results from (31)

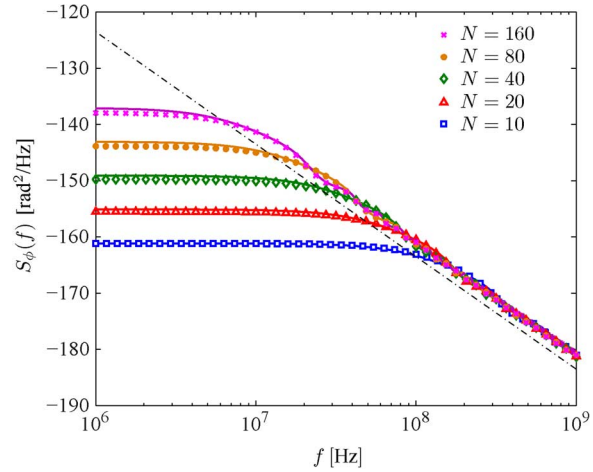

Fig. 9. Phase noise of the PILO oscillator for $W_1 = 320\ \mu$m and for the five values 10, 20, 40, 80, 160 (from bottom to up) of the N multiplication factor: (solid lines) noise from theory, (markers) simulated noise from SpectreRF, (dot-dashed line) noise of free-running oscillator.

are shown as solid lines in the plot. As expected from theory, the noise-filtering bandwidth narrows as the injection frequency is reduced and the ripples in the high-frequency region of the spectrum get closer to each other. Even in this case, the results from SpectreRF (shown as markers in Fig. 9) are in excellent accordance with theory. In this case, the number of harmonics needed in the *pss* and in the *pnoise* analyses must be increased as N. As a result, the simulation time increases significantly at large N values. For instance, for $N = 160$, we need to use 4096 harmonics for the *pss* and 1024 harmonics for the *pnoise*, and the total simulation time to get the phase noise spectrum is of about 12 hours on a quad-core workstation. By contrast, the closed-form expression (31) allows predicting the shapes of the output noise for increasing values of N in a few seconds. The phase noise $S_{\phi_n}(f)$ of the free-running oscillator is also plotted for comparison in Fig. 9. Interestingly, as anticipated at the end of Section IV. the noise spectrum of the PILO exhibits an almost 3 dB increase over free-running phase noise at $f \approx f_{inj}$. This result, which is confirmed by recently presented works [1], contrasts with the common belief that the phase noise of the injection-locked oscillator is identical to that of the free-running oscillator at high-frequency and it is justified by the effect of spectrum folding described in (33).

We conclude this section by verifying the validity of the ansatz exploited in Section IV to transform the nonlinear model (11) into the linearized one (12). To this aim, we simulate in time the nonlinear (11) over a large number of reference cycles and derive the samples of the excess phase $\phi(t_k)$ caused by PILO internal noise sources. Simulated phase values $\phi(t_k)$ result to be Gaussian distributed with a standard deviation of about $2 \cdot 10^{-4}$ rad. For these very tiny fluctuations of $\phi(t_k)$ around the locking value $\theta_{ss} - \theta_{inj} \approx 3.8$ rad (as it can be seen in Fig. 4) the $\gamma(\cdot)$ curve is accurately approximated by a straight line thus validating the overall procedure.

VI. Conclusion

Transistor-level phase-noise simulation of sub-harmonic pulse injection-locked oscillators, and in general of frequency multipliers based on injection locking mechanism, becomes

prohibitively time-consuming as the frequency ratio and the circuit complexity increase. In this paper, we have provided an alternative efficient computational flow to predict phase noise in pulse injection-locked oscillators. The flow relies on calculating the PDR which is able to include in the model the amplitude modulation effects induced by large pulse injection. Starting from the PDR paradigm, we have provided for the first time the nonlinear noise-aware model (11) of the PILO. Since internal noise sources in a PILO are commonly small-amplitude signals, we have shown that this nonlinear model can be linearized around the locking phase condition and that phase-noise can be evaluated with closed-form expressions. The accuracy of the analytical predictions have been verified against detailed SpectreRF simulations in a few significant cases. Finally, an interesting result has been provided that shows how at high frequency the PILO noise spectrum exceeds of almost 3 dB that of the free-running oscillator.

Appendix A

PDR Function Computation

In this appendix, we show how to compute the large-signal phase domain response. We start from the T_0-periodic steady-state response $v_0(t) = p(\omega_0 t)$ of the free-running oscillator. Then, we select arbitrarily a time point over the period and we consider it as the initial time point $t_0 = 0$ for further analysis. Taking as the initial state of the oscillator the state variables evaluated at this time point, we perform the following numerical experiment. A single pulse (whose duration is much shorter than the oscillation period) is applied to the circuit at a time point t_1 with $t_0 < t_1 < T_0$ over the first oscillation cycle. The transient response after the application of this pulse is simulated over a time interval $T_0 \times N$. Fig. 10-(Left) shows, as an example, the response of the PILO circuit $v_{PILO}(t)$ over the first oscillation cycle to a voltage pulse $v_{inj}(t)$ applied at time $t_1 \approx 70$ ps. In this example, the pulse shape is that described in Fig. 3 and the injecting-transistor width is $W_1 = 160\ \mu$m. Comparing $v_{PILO}(t)$ to the free-running response $v_0(t)$, we see that on the first cycle, i.e., where pulse injection occurs, both phase and amplitude variations from the free-running response are significant. Fig. 10-(Right), instead, shows, the two responses over the Nth cycle (in this example $N = 10$), i.e., at the end of reference period: in this case PILO response is simply a time-shifted version of the free-running one, i.e., for $t \gg T_0$

$$v_{PILO}(t) = v_0(t + \Delta t) = p(\omega_0 t + \omega_0 \Delta t). \tag{36}$$

The time shift value Δt is decided by the difference between the zero crossing times (with positive slope) of the two responses. In the example shown in Fig. 10-(right), $\Delta t \approx -25$ ps where the negative sign refers to the fact that PILO response is delayed compared to free-running one. The pulse application time t_1 corresponds to a phase difference value $\theta(t) - \theta_{inj} = \omega_0 \cdot t_1$ in Fig. 4 while the time shift Δt evaluates the PDR function

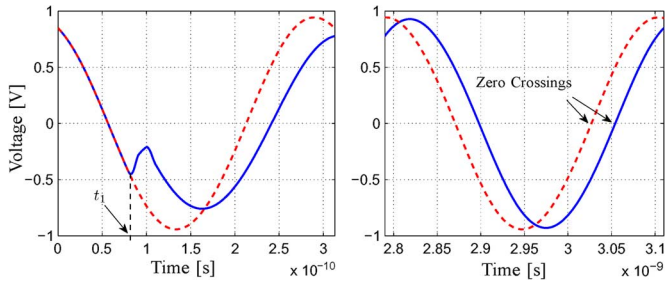

Fig. 10. Output responses: (Left) over the first oscillation cycle, (Right) over the Nth oscillation cycle. (Solid line) PILO response $v_{PILO}(t)$, (Dashed line) free-running response $v_0(t)$.

$\gamma(\theta(t) - \theta_{inj}) = \omega_0 \cdot \Delta t$ in that point. The samples of the $\gamma(\cdot)$ are thus obtained by repeating the above described transient simulation for a sufficiently large number of t_1 values. The numerical simulations needed to extract one such PDR (over 64 samples) shown in Fig. 4 were carried out in a few seconds.

Appendix B

Series Expansion

In this Appendix, we prove that (27) can be simplified into (28). First, we first rewrite (27) in a compact way as

$$T(f) = \frac{\frac{\beta}{T_{inj}} \frac{1}{j2\pi f}}{1 + \frac{\beta}{T_{inj}} D(f)}. \tag{37}$$

with

$$D(f) = T_{inj} \frac{\exp(-j\pi f T_{inj})}{j2\pi} \sum_k \frac{\exp(-j\pi k)}{(f T_{inj} - k)}. \tag{38}$$

Observing that $\exp(-j\pi k) = (-1)^k$ and in view of the following closed-form series expansion (where $a = f T_{in}$)

$$\sum_k \frac{(-1)^k}{(a - k)} = \frac{\pi}{\sin(\pi a)}, \tag{39}$$

we get a simple expression for $D(f)$

$$D(f) = T_{inj} \frac{\exp[-j\pi f T_{inj}]}{2j \cdot \sin(\pi f T_{inj})}. \tag{40}$$

Then, plugging (40) into (37), we find

$$T(f) = \frac{\beta}{j2\pi f T_{inj} + \frac{\pi f T_{inj}}{\sin(\pi f T_{inj})} \beta \exp(-j\pi f T_{inj})}. \tag{41}$$

(28) is obtained from (41) through elementary steps.

References

[1] N. Da Dalt, "An analysis of phase noise in realigned VCOs," *IEEE Trans. Circuits Syst. II, Exp. Briefs*, vol. 61, no. 3, pp. 143–147, Mar. 2014.

[2] S. L. J. Gierkink, "Low-spur, low-phase-noise clock multiplier based on a combination of PLL and recirculating DLL with dual-pulse ring oscillator and self-correcting charge pump," *IEEE J. Solid State Circuits*, vol. 43, no. 12, pp. 2967–2976, Dec. 2008.

[3] B. M. Helal, C. M. Hsu, K. Johnson, and M. H. Perrot, "A low jitter programmable clock multiplier based on a pulse injection-locked oscillator with a highly-digital tuning loop," *IEEE J. Solid State Circuits*, vol. 44, no. 5, pp. 1391–1400, May 2009.

[4] J. Borremans, J. Ryckaert, C. Desset, M. Kuijk, P. Wambacq, and J. Craninckx, "A low-complexity, low-phase-noise, low-voltage phase-aligned ring oscillator in 90 nm digital CMOS," *IEEE J. Solid-State Circuits*, vol. 44, no. 7, pp. 1942–1949, Jul. 2009.

[5] A. S. Landsman and I. B. Schwartz, "Predictions of ultraharmonic oscillations in coupled arrays of limit cycle oscillators," *Phys. Rev. E*, vol. 74, no. 3, pp. (036204)1–(036204)23, Sep. 2006.

[6] A. Palacios et alii, "Multifrequency synthesis using two coupled nonlinear oscillator arrays," *Phys. Rev. E*, vol. 72, no. 1, pp. (026211)1–(026211)9, Aug. 2005.

[7] F. X. Kaertner, "Analysis of white and $f^{-}\alpha$ noise in oscillators," *Int. J. Circuit Theory Appl.*, vol. 18, pp. 485–519, 1990.

[8] A. Demir, A. Mehrotra, and J. Roychowdhury, "Phase noise in oscillators: A unifying theory and numerical methods for characterisation," *IEEE Trans. Circuits Syst. I, Fundam. Theory Appl.*, vol. 47, no. 5, pp. 655–674, May 2000.

[9] A. Hajimiri and T. H. Lee, "A general theory of phase noise in electrical oscillator," *IEEE J. Solid-State Circuits*, vol. 33, pp. 179–194, Feb. 1998.

[10] P. Maffezzoni, "Analysis of oscillator injection locking through phase-domain impulse-response," *IEEE Trans. Circuits Syst. I, Reg. Papers*, vol. 55, no. 5, pp. 1297–1305, Jun. 2008.

[11] F. Ramirez, A. Suarez, S. Sancho, and E. Fernandez, "Nonlinear analysis of pulsed injection-locked oscillators," *Proc. IEEE Int. Microwave Symp. Dig. (MTT)*, pp. 1–3, Jun. 2012.

[12] E. Fernandez, F. Ramirez, A. Suarez, and S. Sancho, "Stability and phase-noise analysis of pulsed injection-locked oscillators," *IEEE Trans. Microwave Theory Tech.*, vol. 61, no. 1, pp. 482–491, Jan. 2013.

[13] D. Pazó and E. Montbrió, "Low-dimensional dynamics of populations of pulse-coupled oscillators," *Phys. Rev. X*, vol. 4, p. 011009, 2014, To appear.

[14] E. M. Izhikevich, *Dynamical Systems in Neuroscience: The Geometry of Excitability and Bursting*. Cambridge, MA, USA: MIT Press, 2007.

[15] D. Dunwell and A. C. Carusone, "Modeling oscillator injection locking using the phase domain response," *IEEE Trans. Circuits Syst. I, Reg. Papers*, vol. 60, no. 11, pp. 2823–2833, Nov. 2013.

[16] A. Demir, "Computing timing jitter from phase noise spectra for oscillators and phase-locked loops with white and $1/f$ noise," *IEEE Trans. Circuits Syst. I, Reg. Papers*, vol. 53, no. 9, pp. 1859–1874, Sep. 2006.

[17] P. Vanassche, G. Gielen, and W. Sansen, "On the difference between two widely publicized methods for analyzing oscillator phase behavior," in *Proc. ICCAD*, Nov. 2002, pp. 229–233.

[18] M. I. Freidlin and A. D. Wentzell, *Random Perturbations of Dynamical Systems*. Berlin, Germany: Springer-Verlag, 1984.

[19] P. Maffezzoni and S. Levantino, "Analysis of VCO phase noise in charge-pump phase-locked loops," *IEEE Trans. Circuits Syst. I, Reg. Papers*, vol. 59, no. 10, pp. 2165–2175, Oct. 2012.

[20] A. Pikovsky, M. Rosenblum, and J. Kurths, *Synchronization*. Cambridge, U.K.: Cambridge Univ. Press, 2001.

[21] Virtuoso Spectre Circuir Simulator RF Analysis User Guide Product Version 7.2, Cadence Design Syst.. San Jose, CA, USA, May 2010.